Traction Network Protection Based on Similarity of Transient Current Waveform

Shilong Chen[1], Zihang Zhang[1], Hao Liu[2], Guihong Bi[1], Chao Xing[3], Pengsong Li[1] and Wenying Zhang[1]*

[1]Department of Electrical Engineering, Kunming University of Science and Technology, Kunming, China, [2]Kunming Power Supply Bureau in Yunnan Power Grid Co., Ltd., Kunming, China, [3]Electric Power Research Institute, Yunnan Power Grid Co., LTD., Kunming, China

In this paper, a protection scheme for the traction network of the penetrating co-phase traction direct power supply system based on the waveform similarity at both ends of line is proposed. Besides, research on the transmission characteristics of fault current is also carried out. This article, from the perspectives of the reflection and refraction process, attenuation degree, and polarity of fault current, analyzes the correlation and difference of current waveforms at both ends when interior line faults and adjacent line faults emerge. The correlation of waveforms can be proved by cosine similarity after the process of synchronous squeezes wavelet transformation of fault current. The conclusions are as follows: when the interior line faults occur, the sequence, reflection and refraction process, and attenuation degree reaching both ends are roughly the same, the polarity change direction is the same, and the waveform similarity is high; when the adjacent line faults occur, the sequence, reflection and refraction process, and attenuation degree reaching at both ends are greatly different, the polarity change direction is opposite, and the waveform similarity is low. When a protection scheme is based on using cosine similarity, it can quickly and accurately identify internal or external current faults. Simulation results show that the proposed algorithm can meet the requirements of rapidity, selectivity, and reliability and is not affected by transition resistance and fault inception angles, so it has an application prospect to a certain degree.

Keywords: penetrating co-phase traction direct power supply system, synchronous squeezed wavelet transformation, cosine similarity, traction network, transient protection

1 INTRODUCTION

The traction direct power supply system is a unique branch of the power system, but suffers high failure frequency due to its complicated deployment environment, such as bad geographic environment, complex weather conditions, locomotive load, and lightning stroke. At the same time, traction network has high requirements for power supply reliability. For this reason, its relay protection scheme must have specific capabilities to quickly and accurately identify the faults.

Relay protection schemes and fault location methods based on traveling wave and transient signals have achieved great success in the deployment of transmission and distribution lines. Deng et al. (2018), Biswas and Milanfar, (2016) and Li et al. (2019) based on time–frequency correlation of fault waveform characteristics put forward a time–frequency matrix constructed by fault waveform of continuous
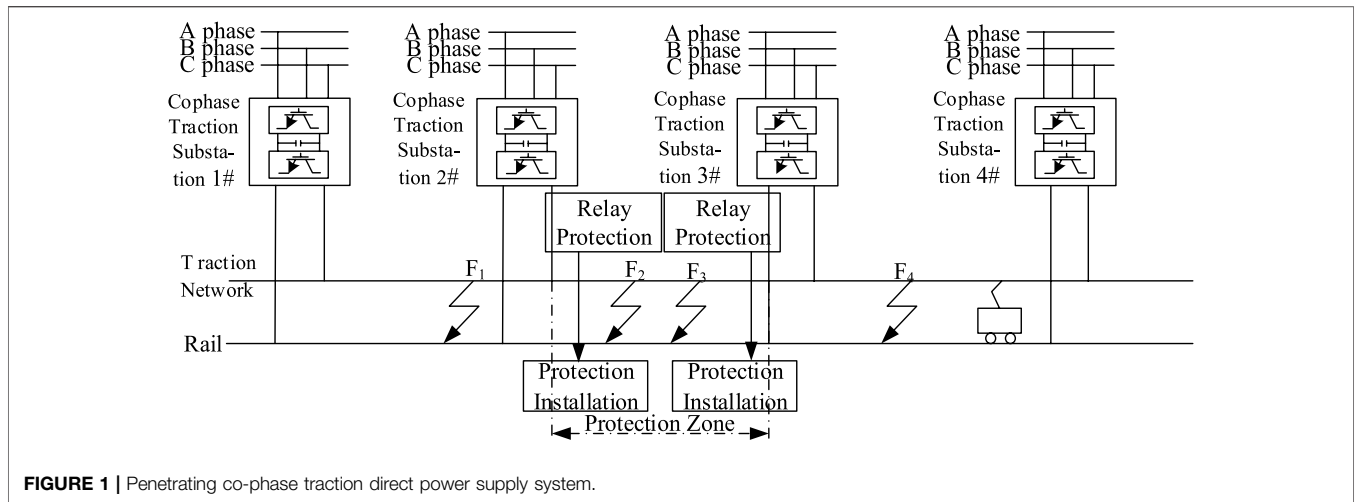
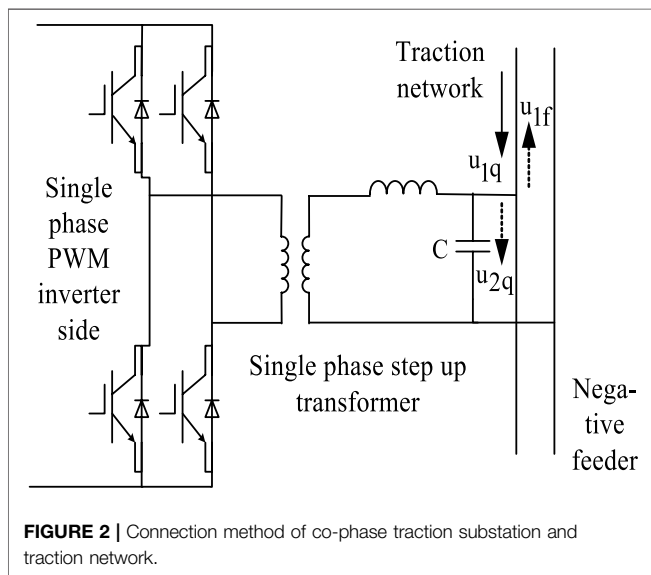**FIGURE 1 |** Penetrating co-phase traction direct power supply system.

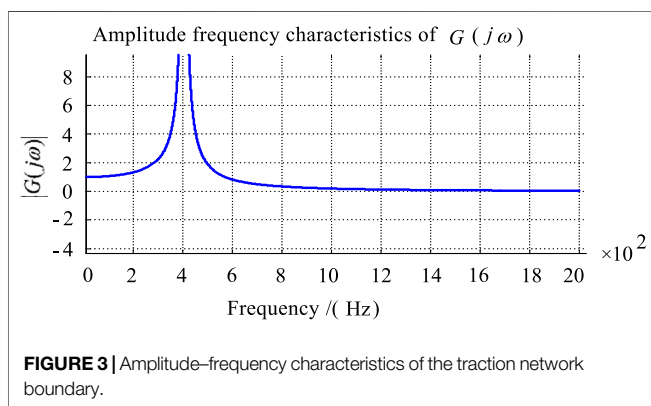**FIGURE 2 |** Connection method of co-phase traction substation and traction network.

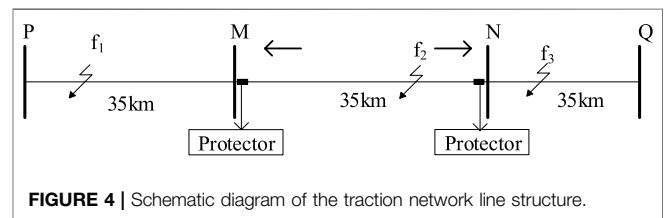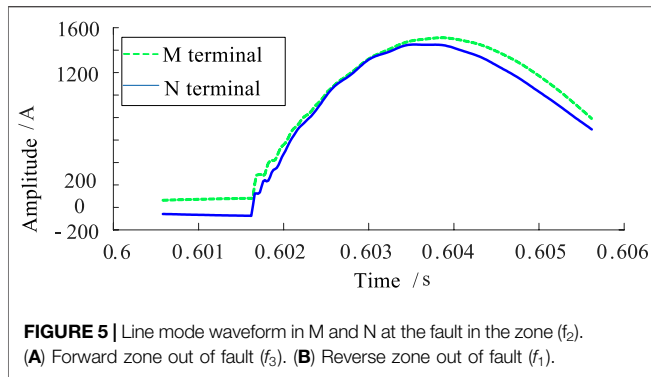**FIGURE 3 |** Amplitude–frequency characteristics of the traction network boundary.

FIGURE 4 | Schematic diagram of the traction network line structure.

the help of cosine similarity of transient current waveform to construct a flexible DC distribution system, give a scheme for outgoing feeder protection of new energy station. Based on the correlation characteristics of fault waveforms, Li Z. et al. (2018) and Hongchun et al. (2012) propose using waveform coefficient to distinguish internal and external faults; Li et al. (2019), based on the waveform similarity of forward and reverse differential currents, state that the fault location information can be accessed by analysis of the Pearson coefficient. In recent years, many researchers in this field have analyzed the propagation characteristics of fault traveling wave in the traction network line and appealed that the research of fault traveling wave and fault located of traction network should be conducted as a whole (Xue et al., 2012; Xiong et al., 2019; Pan et al., 2014). However, fault traveling wave and fault transient signal have not been widely used in the protection of traction network. As transient protection is of the advantages of stability, reliability, and rapidity, it would be a new attempt to apply it to traction network.

The penetrating co-phase traction direct power supply system and capacitance are paralleled at every outlet of traction substations for filtering, and the paralleled capacitance would create wave impedance discontinuity. The waveform detected at the relay location is the transient signal generated by the fault point, and after repeated folding, reflection, (Shen et al., 2021; Shen and Raksincharoensak, 2021a) and refraction, it is superimposed according to a certain time sequence. The traction network and line boundary exert a certain attenuation effect on the fault transient signal, which is why the amplitude of waveform (Shen et al., 2020a; Shen et al., 2020b; Zhang et al., 2021) at both ends of the line is different when the fault location is different. The polarity of the signal detected at both ends of the device is different (Shen and Raksincharoensak, 2021b; Shen et al., 2022) when the fault

wavelet transform and S-transform, and by it, they believe that the internal and external faults of transmission line could be distinguished; Wang et al. (2019) and Zhen et al. (2019), with

FIGURE 5 | Line mode waveform in M and N at the fault in the zone (f_2). (A) Forward zone out of fault (f_3). (B) Reverse zone out of fault (f_1).

forward zone out of fault（f_3）

reverse zone out of fault（f_1）

FIGURE 6 | Line mode waveform in M and N at the fault outside the zone.

location is different. The cosine similarity is used to represent the difference of waveform at both ends of the line. When the information about the reflection and refraction, arrival time sequence, attenuation degree, polarity, and other relevant factors of waveforms at both ends of the line are roughly the same, the waveform similarity is high, and the cosine similarity is large. Otherwise, the cosine similarity is small. Taking advantage of the (Han et al., 2016; Li B. et al., 2018) abovementioned characteristics, the pilot protection of traction network in the traction direct power supply system could be constructed on the basis of the similarity of current waveform.

Synchronous squeeze wavelet transform (SWT) compresses the time–frequency map after wavelet transform in the frequency domain direction (Li et al., 2021; Liu et al., 2020), and its time–frequency curve is clearer and the decomposition result remains approximately unchanged, which is conducive to solving the mode mixing problem and is more accurate than taking wavelet transform, S-transform, and other methods (Duan et al., 2019; Yu et al., 2017a).

This study studies the unique structure of the traction direct power supply system. Based on the transmission characteristics and attenuation function of transient waveform, it analyzed the similarity of the current waveforms at both ends of the traction network interior line faults and adjacent line faults and proposed a new method of the line protection based on synchronous squeeze wavelet and waveform similarity, whereby the internal and external faults can be quickly and accurately identified. The scheme uses cosine similarity of waveform at both ends of the line to form the protection criterion, making effective use of the waveform characteristics and making the protection more reliable, and is not affected by the transition resistance and the initial angle of the fault. It is the first time this method and the traction system have been combined. With the help of simulation software PSCAD/EMTDC, the model of the penetrating co-phase traction direct power supply system could be constructed for effective algorithm verification.

2 STRUCTURE AND BOUNDARY OF THE PENETRATING CO-PHASE TRACTION DIRECT POWER SUPPLY SYSTEM

2.1 Penetrating Co-Phase Traction Direct Power Supply System

The structure of the penetrating co-phase traction direct power supply system is shown in **Figure 1**. The system is mainly
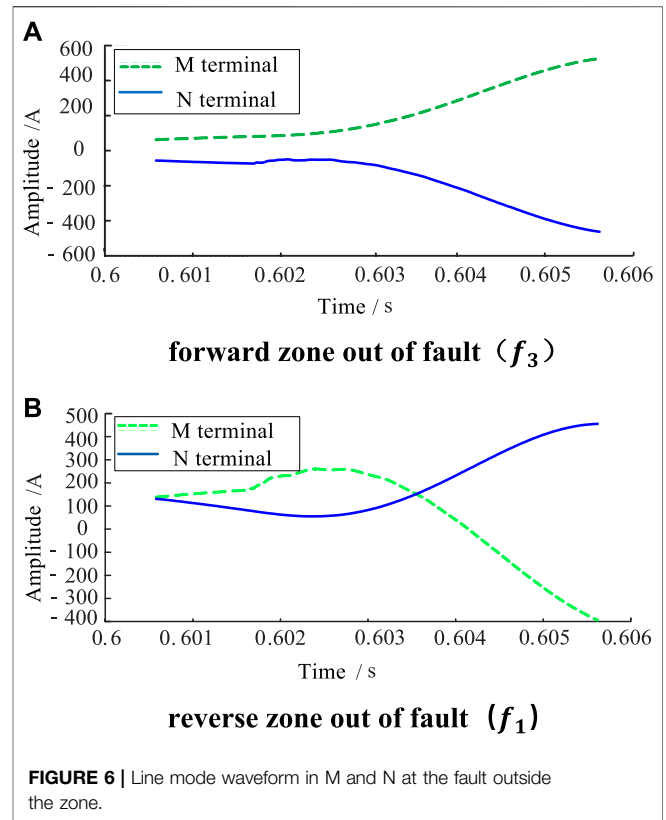
composed of public power grid, traction substation, traction network, and electric locomotive. The three-phase alternating current of the public power grid outputs a single-phase alternating current with equal amplitude and same phase through rectifier operation and inverter operation of traction substation (Li, 2014). Usually, the length of the line between two traction substations is 30–35 km. In this study, 35 km is adopted.

2.2 Boundary of Traction Network

Connection method of co-phase traction substation and traction network is shown in **Figure 2**. The capacitors at the outlet are connected in parallel with the traction network to reduce the harmonic content entering the traction network and improve the power quality of the traction network lines.

The capacitance connected in parallel with traction network shows low impedance to high frequency current. Thus, it is of certain boundary characteristics. When the fault current passes through the boundary of the traction network, a part of the fault current flows into the capacitors, which leads to a sharp difference with the fault current detected at the relay location where internal and external fault appears. According to the method from Song et al., 2014, the capacitance at the outlet of traction substation plus-2 meters contact line is set as the line boundary.

According to the composition of traction network boundary of co-phase traction power supply system, the frequency characteristics are analyzed, as shown in **Figure 3**.

It can be seen from **Figure 3** that fault signals with different frequencies show unequal passage characteristics after passing through the boundary. When the signal frequency is greater than

FIGURE 7 | Protection scheme flowchart.
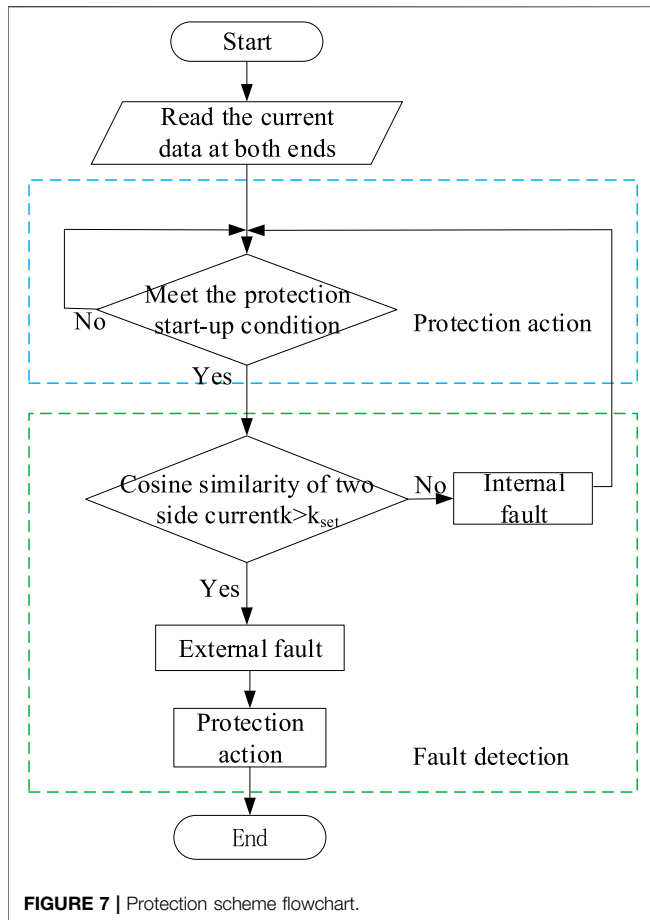
600Hz, the amplitude of amplitude–frequency characteristic is far less than 1, which indicates that the boundary has a strong attenuation effect on high frequency signal (Shen et al., 2017; Yang et al., 2018; Song et al., 2020).

3 THE ANALYSIS OF THE FAULT CURRENT OF THE PENETRATING CO-PHASE TRACTION DIRECT POWER SUPPLY SYSTEM

Figure 4 is the typical schematic diagram of the traction network line structure, and P、Q、M、N is where the traction substation is located, also known as the fault detecting point. In this study, the traction network between M, N is taken as the research object, which is also in the zone. The faults are set in f_1, f_2, and f_3. After the fault occurs in the traction network, the fault transient current signal propagates along the line at the fault point at high speed to both sides, and produces reflection and refraction where the wave impedance is discontinuous. The transient signal detected by the detecting point, M, N, is related to attenuation function, reflection and refraction coefficient and fault location. The positive directions of M、N are shown in **Figure 3**.

3.1 Internal Line Fault

When the fault occurs in f_2 (in the zone), the transient current from the fault point flows to both ends of the line, and the traction network has an attenuation effect on the transient signal of the fault. The polarity changes of the transient current detected by the protection devices at both ends of the line are the same, and the transient current only passes through the line, so the attenuation characteristics, reflection process, and transmission sequence are basically consistent, and the waveform shape of the transient current is basically the same. However, when the fault point is relatively far from the midpoint of the line, the waveform shape is different due to the different arrival time sequence of the fault transient current; at the same time, due to the attenuation effect of the traction network on the fault transient signal, the attenuation degree of the transient current with different frequency is different in the transmission process, so the amplitude is different.

When a metallic short-circuit fault occurs, a distance of 15 km form M, its mode component is obtained by decoupling and transforming the fault transient current of M and N, as shown in **Figure 5**.

It can be seen from **Figure 5** that the waveform of mode component of fault transient current at both ends of the line is basically the same when the fault occurs in the zone.

3.2 Adjacent Line Fault

In case of fault occurring in f_1 (outside the reverse zone) and f_3 (outside the forward zone), the transient current will flow through the boundary of the traction network line, and the waveform of the transient current will be reflected, and the high frequency component will be strongly attenuated when passing through the boundary. The polarity change direction of the current waveform detected by the detecting point, M, N, will be opposite; the reflection and refraction process, attenuation degree, and transmission sequence of the transient current waveform will be completely different. Therefore, the waveform of fault transient current will be completely different.

When a metallic short-circuit fault occurs, a distance of 35 km forms the forward zone of N, that is f_3, its mode component is obtained by decoupling and transforming the fault transient current of M and N, as shown in **Figure 6A**. When a metallic short-circuit fault occurs, a distance of 20 km forms the reverse zone of M, that is f_1, its mode component is shown in **Figure 6B**.

It can be seen from **Figure 6** that the waveform of mode component of fault transient current at both ends of the line is opposite and in sharp difference when the fault occurs outside the zone.

To sum up, the waveform of fault current is related to transmission characteristics (refraction and reflection process, attenuation degree, arrival time sequence, change direction) and transmission function. When the fault occurs in the zone, the refraction and reflection process and attenuation characteristics of the transient current are basically the same, the polarity change direction is the same, and the transmission sequence is slightly different, all resulting in local differences in waveform. But generally speaking, the fault transient current waveforms detected at both ends of the line are basically similar. When the fault occurs outside the area, the transient current attenuates through the boundary, the

Fault location	Fault distance/km	K	Result
f_2 in the zone	0	0.9097	In the zone
	5	0.9214	In the zone
	10	0.9880	In the zone
	15	0.9960	In the zone
	20	0.9967	In the zone
	25	0.9826	In the zone
	30	0.8996	In the zone
	35	0.8749	In the zone
f_3 outside the forward zone	0	−0.8343	Outside the zone
	5	−0.9011	Outside the zone
	10	−0.9816	Outside the zone
	15	−0.9927	Outside the zone
	20	−0.9955	Outside the zone
	25	−0.9965	Outside the zone
	30	−0.9964	Outside the zone
	35	−0.9974	Outside the zone
f_1 outside the reverse zone	0	−0.7751	Outside the zone
	5	−0.8349	Outside the zone
	10	−0.9455	Outside the zone
	15	−0.9683	Outside the zone
	20	−0.9763	Outside the zone
	25	−0.9821	Outside the zone
	30	−0.9885	Outside the zone
	35	−0.9867	Outside the zone

frequency components are different, the refraction and reflection process, the transmission sequence are completely different, and the polarity change direction is opposite. The waveform of fault transient current detected at both ends of the line is significantly different.

4 THE PILOT PROTECTION BASED ON SYNCHRONOUS SQUEEZED WAVELET AND WAVEFORM SIMILARITY

Based on the above analysis, this article puts forward the transmission line protection principle based on the theoretical basis of the change characteristics of current waveform at both ends and the similarity of transient current waveform.

4.1 Similarity Theory

Cosine similarity is widely applied for information retrieval and data mining. In recent years, many scholars have studied, with cosine similarity, the fault line detection, fault location, and line protection (Li B. et al., 2019; Wang et al., 2019; Li Z. et al., 2018). The cosine value of the angle between two vector inner spaces is used to characterize their similarity, which is known as the follows:

$$\cos(\theta) = \frac{\vec{a} \bullet \vec{b}}{\|a\| \times \|b\|} \qquad (1)$$

From **Eq. 1**, it can be concluded that when the direction of two vectors, $\vec{a}$ and $\vec{b}$ are same, cosine similarity is 1; when $\vec{a}$ and $\vec{b}$ are vertical, cosine similarity is 0; when the direction of two vectors, $\vec{a}$ and $\vec{b}$, are opposite, cosine similarity is -1.

If $x = \{x_1, x_2, \cdots, x_n\}$ and $y = \{y_1, y_2, \cdots, y_n\}$ are two independent variables, and n is sampling point, their cosine similarity can be expressed as follows:

$$R(x, y) = \frac{\sum_{i=1}^{n} x_i y_i}{\sqrt{\sum_{i=1}^{n} x_i^2} \sqrt{\sum_{i=1}^{n} y_i^2}}. \qquad (2)$$

In the formula, $R(x, y)$ represents cosine similarity, and x_i, y_i ($i = 1, 2, \cdots, n$) are the No. i element of independent variable, x and y, respectively.

The value range of $R(x, y)$ is [- 1,1], and the sign indicates the relevant direction. For $R(x, y)$, the higher the value, higher the similarity of the waveform of the two signals. When $R(x, y) = -1$, it means that the two signals are completely negatively correlated; when $R(x, y) = 1$, it means that the two signals are completely positively correlated; when $R(x, y) = 0$, the two signals are quite different and uncorrelated (Deng et al., 2018; Li Z. et al., 2018).

4.2 The Method Based on Synchronous Squeezed Wavelet Transformation
4.2.1 Basic Principles of SWT

Daubechies et al., 2011 and Thakur et al., 2013 proposed when obtained by SWT, the time–frequency curve is of higher clearness, the component precision is higher, and the time–frequency energy is more concentrated (Duan et al., 2019; Yu et al., 2017a). In this case, the composite signal, $f(t)$, is as follows:

$$f(t) = \sum_{k=1}^{n} f_k(t) = \sum_{k=1}^{n} A_k(t)e^{-\lambda t} \cos(2\pi\omega_k t + \varphi_k). \qquad (3)$$

TABLE 2 | Cosine similarity under different transition resistances.

Fault location	Transition resistances/ Ω	Fault distance/km	K	Result
f_2 in the zone	0.1	0	0.9097	In the zone
		15	0.9960	In the zone
		35	0.8749	In the zone
	10	0	0.9010	In the zone
		15	0.9954	In the zone
		35	0.8130	In the zone
	50	0	0.8721	In the zone
		15	0.9926	In the zone
		35	0.7980	In the zone
	100	0	0.7542	In the zone
		15	0.9826	In the zone
		35	0.7827	In the zone
f_3 outside of forward zone	0.1	0	−0.9943	Outside the zone
		15	−0.9927	Outside the zone
		35	−0.9974	Outside the zone
	10	0	−0.9078	Outside the zone
		15	−0.9437	Outside the zone
		35	−0.9790	Outside the zone
	50	0	−0.7193	Outside the zone
		15	−0.6853	Outside the zone
		35	−0.6828	Outside the zone
	100	0	−0.7033	Outside the zone
		15	−0.6615	Outside the zone
		35	−0.6553	Outside the zone
f_1 outside the reverse zone	0.1	0	−0.9751	Outside the zone
		15	−0.9683	Outside the zone
		35	−0.9867	Outside the zone
	10	0	−0.7438	Outside the zone
		15	−0.8475	Outside the zone
		35	−0.8359	Outside the zone
	50	0	−0.5858	Outside the zone
		15	−0.5486	Outside the zone
		35	−0.6437	Outside the zone
	100	0	−0.4599	Outside the zone
		15	−0.4235	Outside the zone
		35	−0.4373	Outside the zone

The synchronous squeezed wavelet changes on the basis of continuous wavelet, and $f(t)$ is the change of continuous wavelet transforms into $W_f(a, b)$, in which a, b are the scale and shift factor. The initial estimated instantaneous frequency of $W_f(a, b)$, as a result, is

$$\omega_f(a, b) = \begin{cases} \dfrac{-i}{W_f(a, b)} \cdot \dfrac{\partial\big(W_f(a, b)\big)}{\partial b} \neq 0 \ W_f(a, b) \neq 0 W_f(a, b) = 0 \\ W_f(a, b) = 0 \end{cases} \tag{4}$$

After synchronous squeezing of wavelet coefficient, $W_f(a, b)$, where $\tilde{\varepsilon}$ is the threshold value and accuracy is δ, the result is

$$S_{f,\tilde{\varepsilon}}^{\delta}(b, \omega) = \int_{A_{\tilde{\varepsilon},f}(b)} W_f(a, b) \frac{1}{\delta} h\left(\frac{\omega - \omega_f(a, b)}{\delta}\right) a^{-3/2} da. \tag{5}$$

In this formula, $\tilde{\varepsilon} = 1.4826\sqrt{2 \ln N} \bullet MAD(|W_f|_{n_v})$ and N are the signal length. $MAD(|W_f|_{n_v})$ is the median value of wavelet coefficients in the minimum scale layer; $A_{\tilde{\varepsilon},f}(b) = \{a \in R^+; |W_f(a, b)| > \tilde{\varepsilon}\}$.

If $Z_k = \{(a, b): |a\omega_k'(b) - 1| < \varDelta\}$, when $(a, b) \in Z_k$, there would be

$$\left|\omega_f(a, b) - \omega_k'(b)\right| \leq \tilde{\varepsilon}. \tag{6}$$

After the reconstruction of the component, $f_k(t)$ turns into $\tilde{f}_k(b)$, and the result is as follows:

$$\tilde{f}_k(b) = \lim_{\delta \to 0}\left(R_\psi^{-1} \int_{|\omega - \omega'(b) < \tilde{\varepsilon}|} S_{f,\tilde{\varepsilon}}^{\delta}(b, \omega) d\omega\right). \tag{7}$$
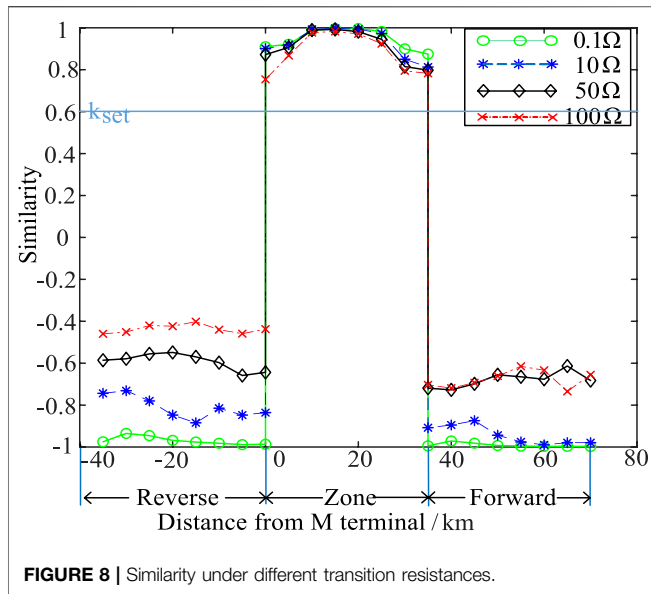
For constant C, if $\forall b \in R$, there would be

FIGURE 8 | Similarity under different transition resistances.

$$\left|\tilde{f}_k(b) - A_k(b)e^{-\lambda b}\cos(2\pi\omega_k b + \varphi_k)\right| \le C\tilde{\varepsilon}. \qquad (8)$$

According to (**8**), the SWT reconstructed component, $\tilde{f}_k(b)$, is very accurately close to composite signal $(f(t))$'s k^{th} component, $f_k(t)$.

4.2.2 The Signal of Synchronous Squeezed Wavelet Transformation Processing

When SWT is used to process fault transient signal, the steps are as follows:

(1) The result of the continuous wavelet transform processing for composite (Yang et al., 2021a; Yang et al., 2021b; Yang et al., 2022) signal, $f(t)$ is as follows:

$$W_f(a, b) = \int_{-\infty}^{+\infty} f(t)a^{-\frac{1}{2}}\bar{\psi}\left(\frac{t - b}{a}\right)dt. \qquad (9)$$

(2) Division of frequency interval: if the length of $f(t)$ is $n = 2^{L+1}$, the sampling interval is Δt, n_v is taken as 32. We assume $n_a = Ln_v$, $\Delta\omega = \frac{1}{n_a-1}\log_2\left(\frac{n}{2}\right)$, and dividing $f(t)$ into different frequency intervals, the lth frequency component of center frequency (ω_l) is as shown in **formula (10)**.

(2) Division of frequency interval: if the length of $f(t)$ is $n = 2^{L+1}$, the sampling interval is Δt, n_v takes 32, $n_a = Ln_v$, $\Delta\omega = \frac{1}{n_a-1}\log_2\left(\frac{n}{2}\right)$ and $f(t)$ is divided into different frequency intervals, as shown in **formula (10)**, the lth frequency component of center frequency (ω_l) would be

$$W_l = \left(\frac{\omega_{l-1} + \omega_l}{2}, \frac{\omega_l + \omega_{l+1}}{2}\right). \qquad (10)$$

.

(3) Computing the coefficient of synchronous squeezed wavelet $(T_f(a, b))$,

$$T_f(\omega_l, b) = (\Delta\omega)^{-1}\sum_{a_k:\,|\omega_f(a,b)-\omega_l|\le\frac{\Delta\omega}{2}} W_f(a, b)a_k^{-\frac{3}{2}}(\Delta a)_k, \qquad (11)$$

where ω_l represents the lth central frequency. a_k is the discrete value of wavelet changing scale, a. $(\Delta a)_k = a_k - a_{k-1}$; $\Delta\omega = \omega_l - \omega_{l-1}$.

(4) After inverse transform, the reconstructed signal, $f(t)$, can be achieved by

$$
\begin{aligned}
f(t) &= \mathrm{Re}\left[C_\psi^{-1}\left(\int_0^{+\infty} W_f(a,b)a^{-3/2}da\right)\right] \\
&= \mathrm{Re}\left[C_\psi^{-1}\left(\sum_i W_f(a,b)a_i^{-3/2}(\Delta a)_i\right)\right] \\
&= \mathrm{Re}\left[C_\psi^{-1}\left(\sum_i T_f(\omega_l,b)(\Delta\omega)\right)\right] \qquad (12)
\end{aligned}
$$

where $C_\psi^{-1} = \int_0^{+\infty}\varphi^*(\xi)\frac{d\xi}{\xi}$ and $\varphi^*(\xi)$ are the conjugated Fourier transform of wavelet function; a_i is the discrete scale; and i is the scale of discreteness.

4.3 Protection Scheme

The basic flow chart of traction network protection algorithm using synchronous squeezed wavelet transformation and waveform similarity is shown in **Figure 7**.

(1) Start
(2) After the procedure has started, the fault transient current under the data window at both ends of the line is collected and decoupled. Selecting a mode component, the reconstructed signal $f(t)$ can be collected after preprocessing of line mode component of current by synchronous squeezed wavelet transformation and then the similarity of waveform at both ends, k is calculated by using the reconstructed signal.
(3) If the similarity between the two ends is greater than the set threshold, $k > k_{set}$, an internal line fault occurs, and protective measures is adopted immediately; otherwise, it is an external line fault and no action is required.

Considering the influence of test error, communication delay, noise and other factors, the constant is set as 0.6, that is, $k_{set} = 0.6$.

5 SIMULATION VERIFICATION AND ANALYZING

With the help of simulation software PSCAD/EMTDC, the model of the penetrating co-phase traction direct power supply system can be constructed, as shown in **Figure 1**.

The line between No.1 and two of traction substation, that is the section of M、N in **Figure 4**, is taken as the research object. As the traction network schematic diagram shown in **Figure 4**, the fault of f_2 (in the zone), f_1 (outside the reverse zone) and f_3, the adjacent line fault (outside the forward zone), are taken into consideration, and the simulation test is carried out, respectively, at different fault locations, different transition

TABLE 3 | Cosine similarity under different fault initial angles.

Fault location	Fault initial angle/(∘)	Fault distance/km	K	Result
f_2 in the zone	5	0	0.8078	In the zone
		15	0.9709	In the zone
		35	0.8940	In the zone
	30	0	0.8088	In the zone
		15	0.9920	In the zone
		35	0.8931	In the zone
	45	0	0.8191	In the zone
		15	0.9955	In the zone
		35	0.8630	In the zone
	90	0	0.9051	In the zone
		15	0.9975	In the zone
		35	0.8935	In the zone
f_3 outside the forward zone	5	0	−0.9893	Outside the zone
		15	−0.9950	Outside the zone
		35	−0.9854	Outside the zone
	30	0	−0.9544	Outside the zone
		15	−0.9942	Outside the zone
		35	−0.9919	Outside the zone
	45	0	−0.8802	Outside the zone
		15	−0.9928	Outside the zone
		35	−0.9903	Outside the zone
	90	0	−0.8810	Outside the zone
		15	−0.9780	Outside the zone
		35	−0.9902	Outside the zone
f_3 outside the forward zone	5	0	−0.8670	Outside the zone
		15	−0.9976	Outside the zone
		35	−0.9666	Outside the zone
	30	0	−0.8596	Outside the zone
		15	−0.9879	Outside the zone
		35	−0.9978	Outside the zone
	45	0	−0.8995	Outside the zone
		15	−0.9642	Outside the zone
		35	−0.9919	Outside the zone
	90	0	−0.8862	Outside the zone
		15	−0.9176	Outside the zone
		35	−0.9680	Outside the zone

resistances, and different fault inception angles. The sampling frequency is set at 50 KHz and the data window, 5 ms.

## 5.1 The Analysis of Internal and External Faults in Different Locations

In order to simulate and analyze the effectiveness of the protection scheme at different fault locations, assuming metal grounding short-circuit faults occur at f_1 (outside the reverse zone), f_2 (in the zone), and f_3 (outside the forward zone), respectively, with the initial fault angle of 60°. Among them, for f_2, starting from 0km, simulated fault points are set every 5 km away from the positive direction of M; for f_3, the right exit of N end is taken as the reference point outside the positive zone, and starting from 0km, simulated fault points are set every 5 km from the positive direction of N; for f_1, the left exit of M end is taken as the reference point outside the negative zone, and starting from 0km, simulated fault points are set every 5 km from the

negative direction of M. After computing the current waveform similarity of M、N at both ends, the results are shown in **Table 1**.

As shown in **Table 1**, in case of fault in the zone, the waveform similarity of both sides of the line is close to 1, indicating that the current waveform on both sides of the line is highly correlated; when the fault occurs outside the zone, value of waveform similarity is close to -1, indicating that the current waveform on both sides is negatively correlated. It can be seen from **Table 1** that the internal and external faults can be accurately identified by the calculation results of cosine similarity.

5.2 The Identification of Internal and External Faults Under Different Transition Resistances

As simulated analysis of effectiveness of the protection scheme, the transition resistances are 0.1Ω, 10Ω, 10Ω, and 100Ω,respectively,

FIGURE 9 | Similarity at different initial fault angles.
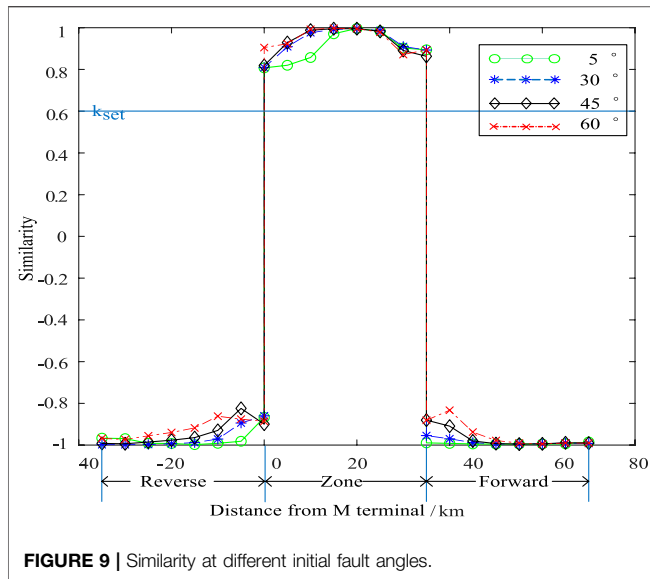
and the initial fault angle is $\theta = 60°$. The setting of fault point is the same as that in **Section 5.1**. The fault current in and outside the zone is detected, and the mode component after phase-mode transformation is taken for synchronous squeezed wavelet transformation, and the similarity of the reconstructed signal can be calculated. Due to limited space, this article provides only the calculation results of waveform similarity at the beginning, midpoint, and end of outside the reverse zone, in the zone, and outside of forward zone under different transition resistance in **Table 2**.

The waveform similarity calculation results of different fault locations under different transition resistances are shown in **Figure 8**.

In **Figure 8**, the abscissa is the distance from the fault point to the protection device, M, and the negative sign indicates the reverse fault; the ordinate is the calculation result of the current waveform similarity of M、N at both ends; the calculation results under different transition resistances are represented by different line types; those parallel to the abscissa are the thresholds (k_{set}) set in this article. It can be seen from **Table 2** and **Figure 8** that under different transition resistances, the similarity of current waveforms at both ends is greater than 0.6 in the case of internal fault, and much less than 0.6 in the case of external fault.

5.3 The Identification of Internal and External Faults at Different Fault Inception Angles

The effectiveness of the protection scheme is analyzed when the fault inception angles are5°,30°,45°, and 90°, respectively, and the transition resistance is 5Ω. Due to limited space, this article only gives the calculation results of waveform similarity at the beginning, midpoint, and end of outside the reverse zone, in the zone, and outside of forward zone at different fault inception angles, as shown in **Table 3**.

The waveform similarity calculation results of different fault locations at different fault inception angles are shown in **Figure 9**.

It can be seen from **Table 3** and **Figure 8** that, at different fault inception angles, the similarity of current waveforms at both ends is greater than 0.6 in the case of internal fault, and much less than 0.6 in the case of external fault.

It can be seen from **Figures 8**, **9** that the similarity value of the fault in the zone is greater than the threshold value, and that of the fault outside the zone is less than the threshold value. When the fault occurs at different initial fault angles, faults can be correctly identified by the protection scheme, which shows that the protection scheme is less affected by the initial fault angle.

From the above simulation results, it can be seen that this protection scheme based on synchronous squeezed wavelet and waveform similarity can accurately identify the internal and external faults when they occur at different fault locations, under different transition resistances, and at different fault initial angles, so as to reliably protect the line.

6 CONCLUSION

In this article, the propagation characteristics of fault transient current in the penetrating co-phase traction power supply system during internal and external faults are analyzed, and a protection scheme for the co-phase traction direct power supply system based on synchronous squeezed wavelet transformation and waveform similarity is proposed. The theoretical analysis and simulation results show the following:

(1) The scheme has the advantages of short time window, easy calculation, and good rapidity
(2) The waveform of fault transient current detected at both ends is basically the same and the polarity change direction is the same as well in the case of internal fault; as for external fault, the waveform of fault transient current detected at both ends is quite different, and the polarity change direction is opposite
(3) The synchronous squeezed wavelet transform can achieve lossless and invertible transformation, and the processed fault transient current can accurately represent the fault information
(4) A large number of simulation experiments show that the protection scheme based on synchronous squeezed wavelet transform and waveform similarity can quickly and accurately distinguish the internal and external faults and can act reliably at different fault locations, under different transition resistances and at different initial fault angles

DATA AVAILABILITY STATEMENT

The original contributions presented in the study are included in the article/Supplementary Material; further inquiries can be directed to the corresponding author.

AUTHOR CONTRIBUTIONS

SC was responsible for methodology, formal analysis, and validation. WZ was responsible for review and supervision and contributed to the conception and design of the study. ZZ was responsible for simulation, data analysis, and manuscript writing. HL and PL wrote sections of the manuscript. GB and CX were responsible for the derivation of the formula. All authors have read and approved the final version.

FUNDING

REFERENCES

Biswas, S. K., and Milanfar, P. (2016). One Shot Detection with Laplacian Object and Fast Matrix Cosine Similarity. *IEEE Trans. Pattern Anal. Mach. Intell.* 38 (3), 546–562. doi:10.1109/tpami.2015.2453950

Daubechies, I., Lu, J., and Wu, H.-T. (2011). Synchrosqueezed Wavelet Transforms: An Empirical Mode Decomposition-like Tool. *Appl. Comput. Harmonic Anal.* 30 (2), 243–261. doi:10.1016/j.acha.2010.08.002

Deng, F., Li, X., Zeng, X., Leng, Y., Ni, J., Ma, S., et al. (2018). Research on Single-End Traveling Wave Based Protection and Fault Location Method Based on Waveform Uniqueness and Feature Matching in the Time and Frequency Domain[J]. *Proc. CSEE* 38 (05), 1475–1487. doi:10.13334/j.0258-8013.pcsee.170899

Duan, J., Li, H., Yang, L., and Zhao, Z. (2019). Transient-based Directional Protection Using Synchrosqueezing Wavelet Transforms for AC Transmission Lines in HVAC/DC Hybrid System[J]. *Proc. CSEE* 39 (13), 3833–3842. doi:10.13334/j.0258-8013.pcsee.180669

Han, L., Zhang, J., and Huang, Z. (2016). Surface Wave Removal with Synchrosqueezing Wavelet Transform[J]. *Oil Geophys. Prospecting* 51 (01), 71–79+19. doi:10.13810/j.cnki.issn.1000-7210.2016.01.010

Hongchun, S., Xincui, T., Jun, D., Guangbin, Z., Yi, Y., and Shiyun, S. (2012). Identification between Internal and External Faults of ±800kV HVDC Transmission Lines Based on Voltage Correlation[J]. *Proc. CSEE* 32 (04), 151–160+5. doi:10.13334/j.0258-8013.pcsee.2012.04.022

Li, B., Zhang, J., Liu, H., and Li, H. (2019). Fault Location of HVDC Transmission Lines Based on Waveform Similarity Analysis[J]. *Electric Power Automation Equipment* 39 (09), 27–32+53. doi:10.16081/j.epae.201909001

Li, B., Qiu, H., Chao, H., Zhang, Y., and Jiang, Y. (2018). High-speed Direction protection of Flexible DC System Based on Voltage Source Converter[J]. *Electric Power Automation Equipment* 38 (02), 1–8. doi:10.16081/j.issn.1006-6047.2018.02.001

Li, Q. (2014). On New Generation Traction Power Supply System and its Key Technologies for Electrification Railway[J]. *J. Southwest Jiaotong Univ.* 49 (04), 559–568. doi:10.3969/j.issn.0258-2724.2014.04.001

Li, Z., He, Z., Guo, T., et al. (2019). Transient Protection Method for Transmission Lines Based on Similarity of Time-Frequency Matrix[J]. *Automation Electric Power Syst.* 43 (05), 121–134. doi:10.7500/AEPS20180806002

Li, Z., Guo, T., Zeng, X., Fan, C., and Xiong, Y. (2018). Wave Correlation Analysis Based Transient Protection Method for Transmission Lines[J]. *Proc. CSU-EPSA* 30 (08), 44–50. doi:10.3969/j.issn.1003-8930.2018.08.008

Li, Z., Jiang, W., Abu-Siada, A., Li, Z., Xu, Y., and Liu, S. (2021). Research on a Composite Voltage and Current Measurement Device for HVDC Networks. *IEEE Trans. Ind. Electron.* 68 (9), 8930–8941. doi:10.1109/tie.2020.3013772

Liu, Y., Yang, N., Dong, B., Wu, L., Yan, J., Shen, X., et al. (2020). Multi-Lateral Participants Decision-Making: A Distribution System Planning Approach with Incomplete Information Game. *IEEE Access* 8, 88933–88950. doi:10.1109/access.2020.2991181

Pan, D., Tian, L., and Zhou, H. (2014). Characteristics of Travelling Wave Propagation in Catenary of High-Speed Railway[J]. *J. China Railway Soc.* 36 (02), 25–30. doi:10.3969/j.issn.1001-8360.2014.02.004

Shen, X., Ouyang, T., Khajorntraidet, C., Li, Y., Li, S., and Zhuang, J. (2022). Mixture Density Networks-Based Knock Simulator. *Ieee/asme Trans. Mechatron.* 27, 159–168. doi:10.1109/TMECH.2021.3059775

Shen, X., Ouyang, T., Yang, N., and Zhuang, J. (2021). Sample-based Neural Approximation Approach for Probabilistic Constrained Programs. *IEEE Trans. Neural Netw. Learn. Syst.*, 1–8. doi:10.1109/TNNLS.2021.3102323

Shen, X., and Raksincharoensak, P. (2021a). Pedestrian-aware Statistical Risk Assessment. *IEEE Trans. Intell. Transport. Syst.*, 1–9. doi:10.1109/TITS.2021.3074522

Shen, X., and Raksincharoensak, P. (2021b). Statistical Models of Near-Accident Event and Pedestrian Behavior at Non-signalized Intersections. *J. Appl. Stat* doi:10.1080/02664763.2021.1962263

Shen, X., Zhang, Y., Sata, K., and Shen, T. (2020a). Gaussian Mixture Model Clustering-based Knock Threshold Learning in Automotive Engines. *IEEE/ASME Trans. Mechatron.* 25 (6), 2981–2991. doi:10.1109/TMECH.2020.3000732

Shen, X., Zhang, X., Ouyang, T., Li, Y., and Raksincharoensak, P. (2020b). Cooperative Comfortable-Driving at Signalized Intersections for Connected and Automated Vehicles. *IEEE Robot. Autom. Lett.* 5 (4), 6247–6254. doi:10.1109/LRA.2020.3014010

Shen, X., Zhang, Y., Shen, T., and Khajorntraidet, C. (2017). Spark advance Self-Optimization with Knock Probability Threshold for Lean-Burn Operation Mode of SI Engine. *Energy* 122, 1–10. doi:10.1016/j.energy.2017.01.065

Song, G., Hou, J., Guo, B., and Chen, Z. (2020). Pilot protection of Hybrid MMC DC Gridbased on Active Detection. *J. Prot. Control. Mod. Power Syst.* V5 (1), 82–96. doi:10.1186/s41601-020-0152-2

Song, G., Ran, M., Xu, C., Jin, X., Liu, T., and Ma, Z. (2014). A New Single-End Current Based Whole-Line Quick-Action Protection for VSC-HVDC Transmission Lines[J]. *Power Syst. Techn.* 38 (05), 1402–1407. doi:10.13335/j.1000-3673.pst.2014.05.043

Thakur, G., Brevdo, E., Fučkar, N. S., and Wu, H.-T. (2013). The Synchrosqueezing Algorithm for Time-Varying Spectral Analysis: Robustness Properties and New Paleoclimate Applications. *Signal. Process.* 93 (5), 1079–1094. doi:10.1016/j.sigpro.2012.11.029

Wang, C., Jia, K., Bi, T., Zhao, Q., and Zhu, R. (2019). Protection for Flexible DC Distribution System Based on Transient Current Waveform Similarity Identification[J]. *Power Syst. Techn.* 43 (10), 3823–3832. doi:10.13335/j.1000-3673.pst.2018.2163

Xiong, L., Wu, G., and Wang, Z. (2019). Study on Fault Location of Multi Measuring Points Traveling Wave Method Based on IHHT in All Parallel at Traction Network[J]. *Trans. China Electrotechnical Soc.* 34 (15), 3244–3252. doi:10.19595/j.cnki.1000-6753.tces.180834

Xue, Y., Duan, J., Xu, B., and Li, J. (2012). Characteristic Analysis of Fault Generated Traveling Waves in Direct Feeding Traction Network[J]. *Power Syst. Techn.* 36 (04), 167–173. doi:10.13335/j.1000-3673.pst.2012.04.041

Yang, N., Ye, D., Zhou, Z., Cui, J., Chen, D., and Wang, X. (2018). Research on Modelling and Solution of Stochastic SCUC under AC Power Flow Constraints. *IET Generation, Transm. Distribution* 12 (15), 3618–3625. doi:10.1049/iet-gtd.2017.1845

Yang, N., Huang, Y., Hou, D., Liu, S., Ye, D., Dong, B., et al. (2019). Adaptive Nonparametric Kernel Density Estimation Approach for Joint Probability Density Function Modeling of Multiple Wind Farms. *Energies* 12, 1356. doi:10.3390/en12071356

Yang, N., Liu, S., Deng, Y., and Xing, C. (2021b). An Improved Robust SCUC Approach Considering Multiple Uncertainty and Correlation. *IEEJ Trans. Elec Electron. Eng.* 16, 21–34. doi:10.1002/tee.23265

Yang, N., Yang, C., Wu, L., Shen, X., Jia, J., Li, Z., et al. (2022). Intelligent Data-Driven Decision-Making Method for Dynamic Multisequence: An E-Seq2Seq-Based SCUC Expert System. *IEEE Trans. Ind. Inf.* 18, 3126–3137. doi:10.1109/TII.2021.3107406

Yang, N., Yang, C., Xing, C., Ye, D., Jia, J., Chen, D., et al. (2021a). Deep Learning-based SCUC Decision-making: An Intelligent Data-driven Approach with Self-learning Capabilities. *IET Generation Trans. Dist* 16, 629–640. doi:10.1049/gtd2.12315

Yu, M., Wang, B., Chen, X., Wang, W., and Jin, J. (2017b). Application of Synchrosqueezed Wavelet Transform for Extraction of the Oscillatory

Parameters of Low Frequency Oscillation in Power Systems[J]. *Trans. China Electrotechnical Soc.* 32 (06), 14–20. doi:10.19595/j.cnki.1000-6753.tces.2017.06.003

Yu, B., Wang, B., Wang, W., Zhang, L., Cheng, Y., et al. (2017a). Power System Time-Varying Transient Harmonics Detection Based on SWT[J]. *Trans. China Electrotechnical Soc.* 32 (S1), 50–57. doi:10.19595/j.cnki.1000-6753.tces.L70483

Zhang, L., Xie, Y., Ye, J., Xue, T., Cheng, J., Li, Z., et al. (2021). Intelligent Frequency Control Strategy Based on Reinforcement Learning of Multi-Objective Collaborative Reward Function. *Front. Energ. Res* doi:10.3389/fenrg.2021.760525

Zhen, L., Jia, K., Bi, T., Fang, Y., and Yang, Z. (2019). Cosine Similarity Based Pilot Protection of Teed Transmission Line Connected to Renewable Energy Power Plants[J]. *Automation Electric Power Syst.* 43 (18), 111–124. doi:10.7500/AEPS20181008011

Conflict of Interest: Authors HL and CX were employed by the company Yunnan Power Grid Co., Ltd.

The remaining authors declare that the research was conducted in the absence of any commercial or financial relationships that could be construed as a potential conflict of interest.

Publisher's Note: All claims expressed in this article are solely those of the authors and do not necessarily represent those of their affiliated organizations, or those of the publisher, the editors, and the reviewers. Any product that may be evaluated in this article, or claim that may be made by its manufacturer, is not guaranteed or endorsed by the publisher.